Eigenvalue and Capacity Analysis Based on Measurement of Massive MIMO System at 3.5 GHZ

Ruijie Xu(✉), Jianhua Zhang, and Jie Xi

Key Lab of Universal Wireless Communications, State Key Lab of Networking and Switching Technology, Ministry of Education, Beijing University of Posts and Telecommunications, P.O. Box 92, Beijing 100876, China
{superjerry1992,jhzhang,xijie}@bupt.edu.cn

Abstract. This paper mainly focus on the analysis of the eigenvalues and capacity for massive multiple-input multiple-output (MIMO) systems based on the channel measurements conducted at 3.5 GHz with 200 MHz. The measurements are conducted under three typical deployment scenarios: the Outdoor to Indoor (O2I), the Urban Macro cell (UMa) and the Urban Micro cell (UMi). Then we investigate the results of the normalized eigenvalues of the channel correlation matrix and angular spread (AS) for both azimuth and elevation direction. Under the line of sight (LoS) condition, the cumulative density function (CDF) of the normalized eigenvalues under O2I has the most uniform distribution followed by UMi, and UMa in the last. The eigenvalues and the orthogonality between sub-channels are affected by the angular spread. The AS of both azimuth and elevation arrival angle under UMi scenario are the biggest, and smallest under UMa. Finally, ergodic capacity for all scenarios is investigated and the advantages of the Massive MIMO system are highlighted. With same signal to noise ratio (SNR), the largest capacity is achieved under UMi in non-line of sight (NLoS) condition.

1 Introduction

Multiple input multiple output (MIMO) has been used in downlink transmission as a must-option in long term evolution (LTE) system. However, with the limits of MIMO channels, to achieve higher data rates is particularly challenging for systems that are power, bandwidth, and complexity limited [1]. Massive MIMO has drawn concern since the concept was firstly introduced by Marzetta [2]. Massive MIMO system takes advantage of multiple transmit and receive antennas, another way significantly increase channel capacity. The basic idea behind massive MIMO is to achieve all the benefits of conventional MIMO on a much larger antenna number scale. Massive MIMO scales conventional MIMO by an order or two in magnitude [3], and extra antennas help by focusing energy into ever smaller regions of space to transmit the signal to desired users and bring

K. Long et al. (Eds.): 5GWN 2017, LNICST 211, pp. 445–458, 2018.
https://doi.org/10.1007/978-3-319-72823-0_42

huge improvements in throughput and radiated energy efficiency by reducing intra-cell interference. Other advantages include extensive use of inexpensive low-power components, reduced latency, simplification of the MAC layer, and robustness against intentional jamming [4].

There has been researches about the massive MIMO system with measurements conducted at 2.6 GHz with 50 MHz [5], the effects on the singular value and capacity of uniform cylindrical array (UCA) and uniform linear array (ULA) antennas at base station (BS) are presented. Some other measurements are conducted at 5.8 GHz with 100 MHz [6] and the analysis mainly focuses on the effect of antenna aperture on frequency dependence. So the propagation characteristics, changing along with the frequency of electromagnetic wave and surrounding environment, play important roles for the performance of the wireless communication systems [7]. One problem worthy of study is that how the massive MIMO system performs under different scenarios at another frequency. Considering 3.5 GHz being a test frequency for the 5th generation wireless communication, we conduct a series of field measurements at 3.5 GHz with 200 MHz. And besides analysing eigenvalues and capacity of the system, we furthermore relate them to the AS.

The distribution of eigenvalues is the most basic property of the channel correlation matrix. It directly represents the spatial correlation of the channel, the number of parallel independent sub-channels that can be used, the multiplexing gain and maximum beam forming gain of massive MIMO system. So another problem worthy of attention is that how the correlation of the sub-channels changes with the number of antennas at BS or mobile station (MS) side changes. With the help of the normalized eigenvalues and the direct observation of the correlation matrix, we will have a more profound understanding. The mean value of the angular spread (AS) shows the degree of freedom (DOF) in the propagation and affects the spatial correlation between the sub-channels. Also the reciprocal of the angular spread is the coherence distance. Finally to evaluate the performance of Massive MIMO system, the capacity results calculated from the real measurement data are compared to the capacity results of simulation for independent identically distributed (i.i.d) channel.

This paper is organized as follows. In Sect. 2, there is the description of both the measurement and the scenarios. The illustration of the data post processing in Sect. 3. Then the analysis of the parameters is given in Sect. 4. Finally, the conclusions are drawn in Sect. 5.

2 Measurement

2.1 Measurement Description

The channel measurements are conducted in Beijing University of Post and Telecommunications, China, utilizing the Elektrobit Propsound Sounder described. Three measurements scenarios are the O2I scenario, the UMa scenario and the UMi scenario. The massive MIMO system considered is that of 128 antenna elements at the BS side and 32 antenna elements at the MS side.

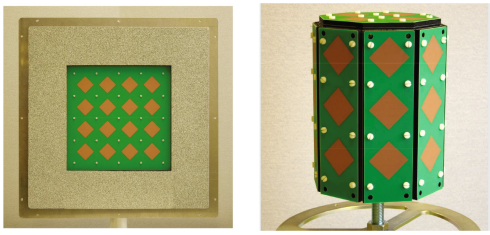

(a) Layout of UPA at MS (b) Layout of ODA at MS

Fig. 1. Layout of antennas

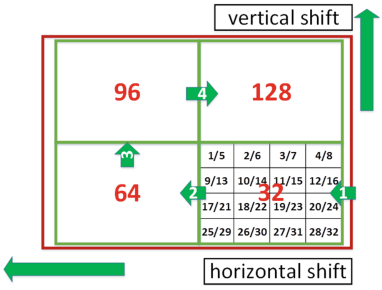

Fig. 2. Illustration of the virtual uniform planar array

At the BS side, the inter element spacing is defined as d and it is fixed on $\lambda/2$ (λ refers to the wave length) for both the horizonal and elevational direction. In the literature [8], it is shown that mutual coupling among antenna elements will have an impact on the system capacity when $d \leq 0.2\lambda$ (Fig. 2).

The layout of the antenna arrays at BS and MS side is illustrated in Fig. 1. Two dual-polarized omnidirectional array (ODA) consisting of 16 antenna elements with 8 adjacent sides and a top surface were used at the MS side. At the BS side, there is a dual-polarized uniform planar array (UPA) with 32 antenna elements. In order to meet the requirement, the UPA is moved to four different position to form a virtual uniform planar array with 128 antenna elements. The rationality of the virtual measurement was proved in [9]. The configuration of the antenna arrays along with other measurement parameters are shown in Table. 1.

2.2 Scenario Description

For the UMi scenario, a residential quarter inside the campus is chosen, a typical one. The concrete scenario is illustrated in Fig. 3. The UPA is set on a building with a height of 14.4 m as shown in Fig. 3(a). The mobile MS is located on nine positions of the streets around the building, which are shown in Fig. 3(b), covering both the line of sight (LoS) and non line of sight (NLoS) conditions. When it comes to the UMa scenario, the UPA is set on the rooftop of the main teaching building with 71 m height. The positions for MS are chosen around the

Table 1. The specifications of measurement

Parameter		Value	
Antenna type		ODA (MS)	UPA (BS)
Number of antenna ports		32	32
Number of elements		8 dual polarized	16 dual polarized
Polarized		±45°	±45°
Angle range	Azimuth	−180° ∼ 180°	−70° ∼ 70°
	Elevation	−70° ∼ 90°	−70° ∼ 70°
Center frequency		3.5 GHz	
Band width		200 MHz	
TX power	UMi	32.1 dBm	
	O2I	31.1 dBm	
	UMa	32.8 dBm	
PN sequence		127 chips (UMi, O2I), 255 chips (UMa)	

(a) BS Position for UMi (b) MS Position for UMi

Fig. 3. Illustration of UMi scenario

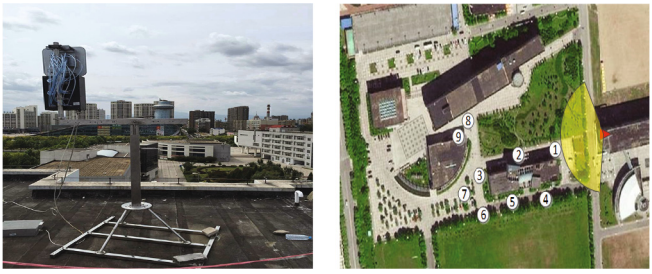

(a) BS Position for UMa (b) MS Position for UMa

Fig. 4. Illustration of UMa scenario

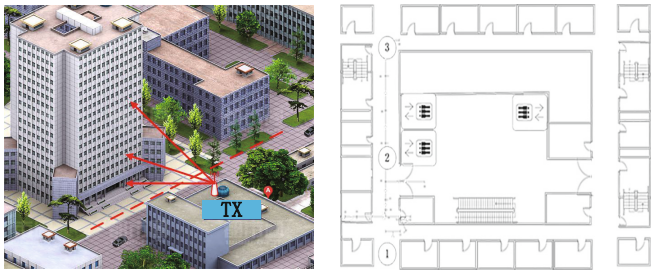

(a) BS Position for O2I (b) MS Position for O2I

Fig. 5. Illustration of O2I scenario

building right in front of the main teaching building to cover both the LoS and NLoS conditions. Figure 4 is for the illustration. Finally, for the O2I scenario, the UPA is on the rooftop of the no. 1 teaching building of a height of 13.4m. The MS are planned to be on the 4th floor with a height of 14.4 m and 7th floor with a height of 26 m in the building shown in Fig. 5(a). The floor plan display is shown in Fig. 5(b). Detailed values of the scenarios are shown in Table. 2.

Table 2. The specifications of scenario

Scenario	UMi	UMa	O2I 4th floor	O2I 7th floor
Height of UPA (m)	14.4	71	13.4	13.4
Height of ODA (m)	1.9	1.9	14.4	26.0
Parameter	Horizontal distance (m) BS to MS			
Pos1	28	58	28	28
Pos2	27.5	97	28	28
Pos3	51	154	28	28
Pos4	74.5	78	-	-
Pos5	75	101	-	-
Pos6	72.5	149	-	-
Pos7	29	172	-	-
Pos8	48	167	-	-
Pos9	58	-	-	-

3 Data Processing

Measurement data acquired using Elektrobit Propsound sounder [10] enables us to analyze how the massive MIMO system performs. After getting the channel impulse response (CIR) from the original data, the frequency response can be acquired.

3.1 Eigenvalue

$H(j,k)_{M,N}$ is defined as a discrete sample of the CIR matrix $H(t,f)_{M,N}$, which can be written as

$$\begin{aligned} H_{M,N}(j,k) &= H_{M,N}(t,f)|_{t=j\cdot\Delta t, f=k\cdot\Delta f} \\ &= H(j\cdot\Delta t, k\cdot\Delta f) \end{aligned} \tag{1}$$

where the row number M is the number of the transmitter antenna and the column number N is the number of the antenna at the receiver side. And Δt and Δf respectively represent discrete interval in the time domain and frequency domain. $H(j,k)_{M,N}$ is the form of the CIR matrix after fast fourier transformation (FFT). To the CIR matrix at moment j and frequency point k, the singular value decomposition (SVD) of it can be written as

$$\begin{aligned} H(j,k) &= U_{SVD}(j,k)\sum(j,k)V_{SVD}^{T}(j,k) \\ &= \sum_{i=1}^{r}\xi_i(j,k)u_i(j,k)v_i(j,k) \end{aligned} \tag{2}$$

$1 \le r \le \min(M,N)$ refers to the rank of the channel impulse response matrix at moment j and frequency point k. ξ_i is the ith biggest singular value of matrix $H(j,k)$. The distribution of eigenvalues of channel correlation matrix plays a very important role for the performance analysis of MIMO transmission systems. When calculating the channel correlation matrix from the BS side, it is defined as

$$R(j) = E\left\{H(j,k)_{M,N}H^{T}(j,k)_{M,N}\right\} = E\left\{R(j,k)\right\} \tag{3}$$

$R(j)$ is the average of all the correlation matrix $R(j,k)$ by dimension k.

$$R(j) = U\Lambda U^{T} \tag{4}$$

So $\xi_i = \sqrt{\lambda(i)}$, $\lambda(i)$ is the ith biggest eigenvalue of the channel correlation matrix. Then CDF of the normalized eigenvalues can be written by

$$\begin{aligned} F(l) = \sum_{1\le l\le i}\lambda(l) \Big\backslash \sum_{1\le l\le rank(h(t,f)_{M,N})}\lambda(l) \\ (i = 1,2,...,rank(H(j,k)_{M,N})) \end{aligned} \tag{5}$$

3.2 Angular Spread (AS)

Root mean square angle spread σ_{AS} can reflect the dispersion of the propagation path gain in the spatial domain, that is, the two order statistics. The mean angle spread μ and the circular angle spread (CAS) σ_{AS} can be calculated by [11]. The concept of CAS is adopted to avoid the angle ambiguity problem.

$$\mu(\Delta) = \frac{\sum_{m=1}^{M}\phi_m(\Delta)P_m}{\sum_{m=1}^{M}P_m} \tag{6}$$

$$\sigma_{AS} = \sqrt{\frac{\sum_{m=1}^{M} (\phi_m - \mu(\Delta))^2 P_m}{\sum_{m=1}^{M} P_m}} \tag{7}$$

$$\phi_m(\Delta) = \phi_m + \Delta \tag{8}$$

$$\phi_m = \begin{cases} 2\pi + \phi_m & \phi_m < -\pi \\ \phi_m & |\phi_m| \leq \pi \\ 2\pi - \phi_m & \phi_m > \pi \end{cases} \tag{9}$$

where M, P_m, and $\phi_m(\Delta)$ denote the number of paths, the power of the mth path and the angle of the mth path adding a shifted angle which denotes a certain angular shift. To get the angular spread, the CIR is processed with the SAGE algorithm [12] to extract the above parameters. Then the angular spread σ_{AS} can be calculated by Eq. 6.

3.3 Capacity

Channel capacity of the jth time index can be caculated by [13]

$$C(j) = \frac{1}{K} \sum_{k=1}^{K} \log_2 \det \left(I_N + \frac{\rho}{\beta M} H_{M,N}(j;k) \, {H_{M,N}}^H(j;k) \right) \tag{10}$$

where ρ is the signal-to-noise ratio (SNR) and β is a common normalization factor to remove the effects of pathloss, defined by

$$\mathrm{E}\left[\frac{1}{\beta} \left\| H_{M,N}(j;k) \right\|_F^2 \right] = M \cdot N \tag{11}$$

4 Analysis of the Measurement Results

4.1 Eigenvalues

The antenna number of the BS side is denoted as N_{bs} and $N_{bs} = 128$. The antenna number of the mobile station is denoted as N_{ms}. We study the normalized eigenvalues of one mobile station for two cases: case1-$N_{ms} = 4$ and case2-$N_{ms} = 16$. And we display the result with the LoS condition under the UMi scenario in Fig. 6. So for the case2, the number of the sub-carrier are definitely more than that of case1. The main eigenvalues are emphatically focused, especially the largest eigenvalue. Taking 0.5 CDF value as an example, the largest eigenvalue of case2 is smaller than that of case1 by 0.1 for sum ratio. The distribution of main eigenvalues is also more concentrated. From Fig. 6, we can see that for case1 the first two eigenvalues count for over 90% of the whole, while for case2 seven eigenvalues count the same. The largest eigenvalue referred to the path with the best transmitting ability and the main eigenvalues referred to the paths that make a major contribution in the Massive MIMO system performance. As the transmitting power staying unchanged, the main eigenvalues

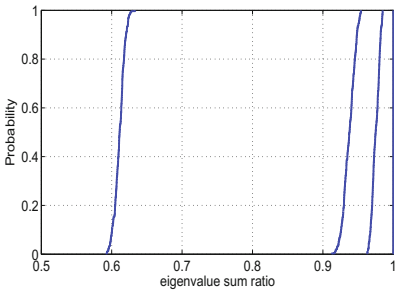

(a) Case1

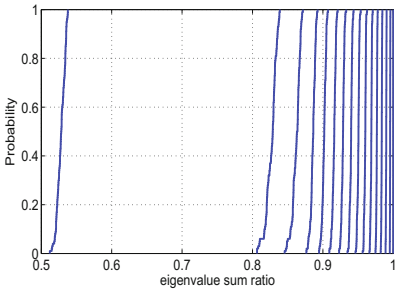

(b) Case2

Fig. 6. The normalized eigenvalues of different antenna numbers of one MS

decrease as the power is more evenly allocated to each sub channel and more paths are contributing. Thus in the picture the level of dispersion grows, however, the speed of growth gets slower as the number of MS antennas growing from 8 to 128.

Then the comparison for the orthogonality of the antennas at the MS side is displayed in Fig. 7. Here, we define the orthogonality of the mobile stations as $O_{ant1,ant2}$:

$$O_{ant1,ant2} = \frac{1}{\rho_{ant1,ant2}} \tag{12}$$

$\rho_{ant1,ant2}$ denotes the correlation between the antennas at the MS side, $ant1, ant2$ refers to the antenna index. As mentioned in Sect. 2, there are two ODAs each with 16 antennas as two mobile stations. One ODA has antennas with the indices from 1 to 16 and connected to the ports with the same indices on the ODA. Another ODA with antenna indices from 17 to 32 also has the antennas connected to ports from 1 to 16. For the two ODA, the antenna pair consisting of antenna 1 and 2 or antenna 17 and 18 facing directly to the UPA, which means that these antennas correspond to the main sub-channels when under LoS condition. The two mobile stations are placed at symmetric positions to the receiver with a interval-$d_{ms} = 20\lambda$. The examples in Fig. 7(a) and (b) show the orthogonality between the antennas with indices: 1, 2, 17, 18 with the LoS

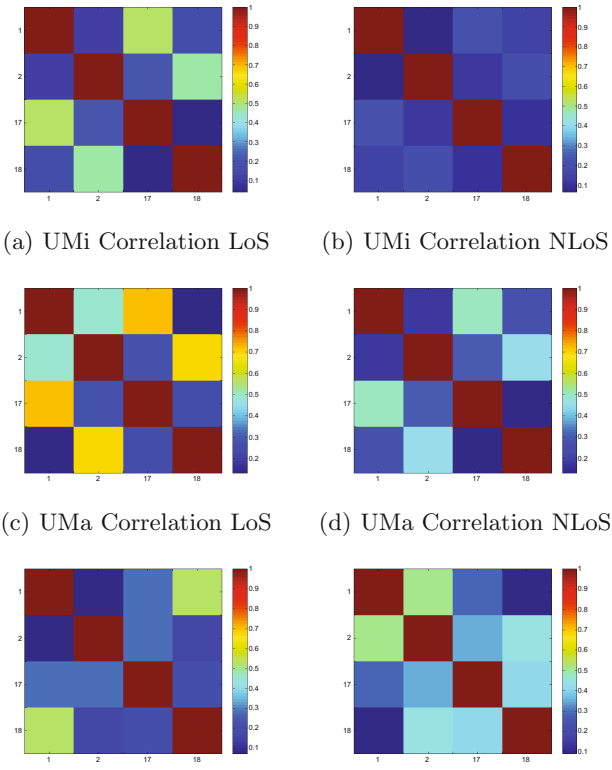

(a) UMi Correlation LoS (b) UMi Correlation NLoS

(c) UMa Correlation LoS (d) UMa Correlation NLoS

(e) O2I Correlation LoS (f) O2I Correlation NLoS

Fig. 7. Correlation of the users

condition and NLoS condition under the UMi scenario. In Fig. 7(c) and (d) the corresponding results under the UMa scenario are shown. For the LoS condition under the UMi scenario, the orthogonality between antenna1 and antenna 17 is the lowest than that of other antenna combination of antenna1 or antenna17, with $O_{1,17} = 1.8$, while the highest orthogonality woulde be $O_{17,18} > 10$. Then as a comparison, with NLoS condition, $O_{ant1,ant2} > 5$ for any two antennas. A similar phenomenon that can be observed for the UMa scenario. So orthogonality between antennas increases when changing from LoS condition to NLoS condition. However, when it comes to the O2I scenario, the results shown in Fig. 7(e) and (f) become irregular due to the shadow fading which leads to a random scattering environment. So considering the narrow space, the affect of space interval between the two ODAs counts more when compared to other scenarios.

Then considering case3-N_{bs} changes and the receive antenna number remains fixed. Four antenna elements of one mobile station are chosen. For all scenarios, we picked the measurment location with the LoS condition and results of a configuration with three kind of BS antenna element numbers are shown in Fig. 8.

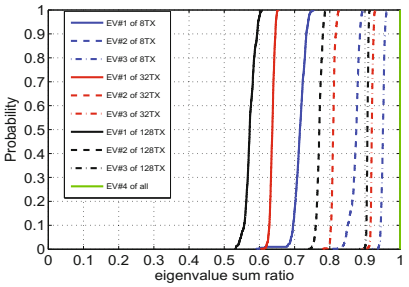

(a) O2I(200M)

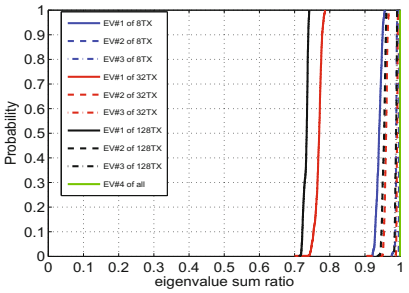

(b) UMa(200M)

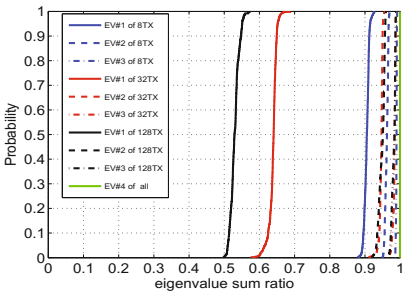

(c) UMi(200M)

Fig. 8. Main eigenvalue for different scenarios

In case3, as N_{bs} grows, similar law appears in the CDF of the normalized eigenvalues as N_{ms} grows. Besides, we can see the difference between the CDF of the normalized eigenvalues under different scenarios. The largest eigenvalue under the UMa scenario is the biggest among the three scenarios and the eigenvalue distribution is also the most dispersed. Then for UMi and O2I scenario, when $N_{bs} = 32/128$, the largest eigenvalues are almost the same meaning that the power of LoS path for the two scenarios are close. However, the O2I scenario have other three resolvable paths while the UMi scenario have another strong path, thus the power allocation is more uniform under the O2I scenario.

But when $N_{bs} = 8$, there is mainly one LoS path for both UMi and UMa as only 8 antennas take use of part of the space. With more antennas at the BS side, the size of the antenna array is larger and makes better use of the space.

Comparing the results of cases with antenna numbers changing whether at the BS side or the MS side, the main eigenvalue distribution of the less antenna numbers is relatively dispersed, which indicates that most of the energy of the channel is mainly distributed in one sub channel. Because the energy of other sub channels is weak, the data transmission ability is poor and unstable to interference. In this way, the multiplexing gain of the whole channel is limited and the spatial correlation of the channel is relatively high. One testification has been drawn from the result that no mater how large the number of antennas grows, the largest 2–4 eigenvalues occupy more than 60% of the whole.

4.2 Angular Spread (AS)

From the values of the azimuth angle spread of arrival (AASA) shown in Table 3, azimuth angle spread of departure (AASD), elevation angle spread of arrival (EASA), elevation angle spread of departure (EASD), we can see that UMa scenario gets the smallest AASA and EASA with LoS condition, while the UMi scenario gets the largest. To explain this, we go to the illustration picture Fig. 4, we can see that under the UMa scenario, due to a broad space and geographical location in the suburbs, there is not much scatterers such as: pedestrians, vehicles between the UPA and ODA, only some of the sparse distributed tall buildings. Then compared to the UMa scenario, the UMi scenario gets densely distributed pedestrians, vehicles and tall buildings around on, as a result, the mobile stations face a much richer scattering environment. Due to a richer scattering environment, the degree of dispersion of energy increases and brings bigger AS, so the AS of arrival for both horizon and elevation plane under UMi scenario are the largest. With bigger AS, there is a bigger DOF [14] meaning lower spatial correlation for the sub-channels. Then we have more concentrated eigenvalue as Fig. 8 displays.

Table 3. AS ($N_{bs} = 32$) for LoS condition under all scenarios

Scenario	Variable	UMi	UMa	O2I
AASA(lg(°))	μ_σ	1.7524	0.76616	1.54042
	ε_σ	0.0473	0.1643	0.0412
AASD(lg(°))	μ_σ	1.12561	1.37954	1.38654
	ε_σ	0.0818	0.0394	0.0536
EASA(lg(°))	μ_σ	1.59731	1.06604	1.33906
	ε_σ	0.0243	0.0616	0.0698
EASD(lg(°))	μ_σ	1.46058	1.42876	1.418
	ε_σ	0.0445	0.0161	0.0256

As for the O2I scenario, the MSs are placed indoor and on different floors. Walls, doors, rooms and other objects in the building on the specific floor contribute as the scatters. Compared to the UMi scenario, the distribution of the scatterer for the MS mainly changes on the elevation direction. Thus, with the LoS condition, there is the LoS path directly from the BS to the antenna of the MS facing to the UPA dominating the channel. The power of the strongest sub-channel depends on the propagation distance. And we pcik the measurement data of position2 of the UMi scenario and position1 on the 4th floor of the O2I scenario to analysis. Figure 3(b) shows the concrete scene for position2 of the UMi scenario. The horizontal distances are both 28 m and the propagation distances are very close. So as Fig. 8 shows, the largest eigenvalue are almost the same. However, the distribution of the 2th, 3rd, 4th eigenvalue is more uniform than that of the UMi scenario. As an explanation, we can see that the 1st and 2nd strongest paths can directly arrive at the MS side under the UMi scenario, so compared to other paths, the power of the 1st, 2nd paths are much stronger. But under the O2I scenario, the 1st stongest path can pass through the windows, while the 2nd, 3rd, 4th paths pass through walls, rooms and doors and get weaker.

4.3 Capacity

Capacity for different scenarios with a configuration of 128 antennas at the BS side and 32 antennas at the MS side and for the i.i.d channel is shown in Fig. 9. From the picture, we can see that under one scenario, capacity for NLoS condition is bigger than that for LoS condition and better SNR improve more capacity for NLoS condition than LoS condition. The capacity for i.i.d channel with an antenna configuration of 128 transmitting antennas and 32 receiving antennas and another antenna configuration of 8 transmitting antennas and 8 receiving antennas as a typical conventional MIMO system are displayed. Taking SNR = 15 dB, the capacity under UMi scenario and NLoS condition, C = 100 bps/Hz,

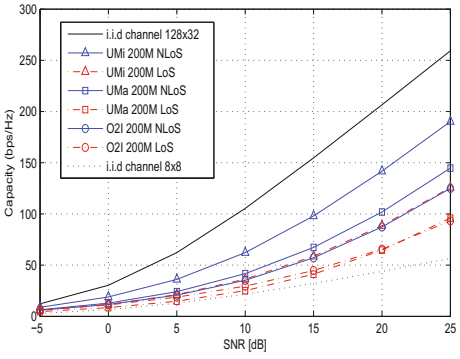

Fig. 9. Capacity

approaches that of the 128×32 i.i.d channel the most closely. However, the difference is still impressive as the capacity gap is almost 50 bps/Hz. So increasing the number of BS or MS antenna elements can still help improve the practical capacity of the multiuser MIMO system [15]. But over all, the performance of the massive MIMO system is even better than the ideally achieved capacity of the conventional MIMO system.

5 Conclusion

Based on the measurement data, we study that how the distribution of eigenvalues changes for three cases. Case1: a growing receiving antenna number. From result, it can be seen that orthogonality between the users increased. So distinguishing the user will be easier. Case2: the growing number at the BS side. And we see that more transmitting antennas will bring bigger multiplexing gain and deteriorative spatial correlation between the sub-channels. Case3: different propagation characteristics. We see that a richer scattering environment can also reduce the spatial correlation and improve the system performance.

After getting the result of AS, it is explained by analyzing the scenarios. So the AS can reflect the effect of propagation characteristics on spatial correlation. Finally, we display the real capacity under different scenarios and comparison to the i.i.d channels. According to the result of performance, the massive MIMO system do have its advantages at the frequency 3.5 GHz, but the gap to ideal channel performance shows us there is still a lot of work to do to accomplish the 5G goal of providing higher capacity.

Acknowledgment. This research is supported in part by National Science and Technology Major Project of the Ministry of Science and Technology (2015ZX03002008), and in part by MOE-CMCC 1-5, and in part by National Natural Science Foundation of China (61322110, 61461136002), and by 863 Program (2015AA01A703) and Doctoral Fund of Ministry of Education (20130005110001). The authors would also like to thank the support from the Huawei Technologies Co., Ltd.

References

1. Goldsmith, A., Jafar, S.A., Jindal, N., et al.: Capacity limits of MIMO channels. IEEE J. Sel. Areas Commun. **21**(5), 684–702 (2006)
2. Marzetta, T.L.: Noncooperative cellular wireless with unlimited numbers of base station antennas. IEEE Trans. Wirel. Commun. **9**(11), 3590–3600 (2010)
3. Rusek, F., Persson, D., Lau, B.K., et al.: Scaling up MIMO: opportunities and challenges with very large arrays. IEEE Sign. Process. Mag. **30**(1), 40–60 (2012)
4. Larsson, E., Edfors, O., Tufvesson, F., et al.: Massive MIMO for next generation wireless systems. IEEE Commun. Mag. **52**(2), 186–195 (2014)
5. Gao, X., Edfors, O., Rusek, F., et al.: Massive MIMO performance evaluation based on measured propagation data. IEEE Trans. Wirel. Commun. **14**(7), 1–1 (2015)
6. Martinez, A.O., Carvalho, E.D., Nielsen, J.O., et al.: Frequency dependence of measured massive MIMO channel properties. In: IEEE Vehicular Technology Conference (2016)

7. Goldsmith, A.: Wireless Communications. Stanford University, California (2008)
8. Liu, X., Bialkowski, M.E.: Effect of antenna mutual coupling on MIMO channel estimation and capacity. Int. J. Antennas Propag. **2010**(6), 252–260 (2010)
9. Yu, H., Zhang, J.H., Zheng, Q., et al.: The rationality analysis of massive MIMO virtual measurement at 3.5 GHz. In: IEEE/CIC International Conference on Communications in China (2016)
10. Zhang, J.H.: Review of wideband MIMO channel measurement and modeling for IMT-advanced systems. Sci. Bullet. **57**(19), 2387–2400 (2012)
11. Rappaport, T.S.: Wireless Communications: Principles and Practice, 2nd edn. Prentice Hall, Upper Saddle River (2001)
12. Fleury, B.H., Tschudin, M., Heddergott, R., et al.: Channel parameter estimation in mobile radio environments using the SAGE algorithm. IEEE J. Sel. Areas Commun. **17**(3), 434–450 (1999)
13. Heath, R.W., Paulraj, A.J.: Switching between diversity and multiplexing in MIMO systems[J]. IEEE Trans. Commun. **53**(6), 962–968 (2005)
14. Gesbert, D., Kountouris, M., Heath, R.W., et al.: Shifting the MIMO paradigm. IEEE Sign. Process. Mag. **24**(5), 36–46 (2007)
15. Zhang, J.H., Pan, C., Pei, F., et al.: Three-dimensional fading channel models: a survey of elevation angle research. IEEE Commun. Mag. **52**(6), 218–226 (2014)